# CCL2-Mediated Reversal of Impaired Skin Wound Healing in Diabetic Mice by Normalization of Neovascularization and Collagen Accumulation

Yuko Ishida[1], Yumi Kuninaka[1], Mizuho Nosaka[1], Machi Furuta[2], Akihiko Kimura[1], Akira Taruya[3], Hiroki Yamamoto[1], Emi Shimada[1], Mariko Akiyama[4], Naofumi Mukaida[4] and Toshikazu Kondo[1]

Patients with diabetes frequently present with complications such as impaired skin wound healing. Skin wound sites display a markedly enhanced expression of CCL2, a potent macrophage chemoattractant, together with macrophage infiltration during the early inflammatory phase in skin wound healing of healthy individuals, but the association of CCL2 with delayed skin wound healing in patients with diabetes remains elusive. In this study, we showed that, compared with control mice, mice with streptozotocin-induced diabetes displayed impaired healing after excisional skin injury, with decreased neovascularization, CCL2 expression, and macrophage infiltration. Compromised skin wound healing in mice with diabetes was reversed by the administration of topical CCL2 immediately after the injury, as evidenced by normalization of wound closure rates, neovascularization, collagen accumulation, and infiltration of macrophages expressing vascular endothelial growth factor, a potent angiogenic factor, and transforming growth factor-β. CCL2 treatment further increased the accumulation of endothelial progenitor cells at the wound sites of mice with diabetes and eventually accelerated neovascularization. Thus, the topical application of CCL2 can be an effective therapeutic option for the treatment of patients with diabetes with defective wound repair, promoting neovascularization and collagen accumulation at skin wound sites.

*Journal of Investigative Dermatology* (2019) **139,** 2517–2527; doi:10.1016/j.jid.2019.05.022

## INTRODUCTION

Inflammation is the first stage of wound repair, which is initiated by clotting at the site of tissue injury and the subsequent release of platelets and neutrophils. Subsequently, macrophages infiltrate to clear debris from the wound. Chemokines play an important role in the normal wound healing process by regulating the spatiotemporal recruitment of distinct types of leukocytes (Ochoa et al., 2007b; Singer and Clark, 1999). With cytokine and growth factor secretion, recruited leukocytes can promote the next stage of wound repair, the proliferative stage, which is characterized by granulation tissue formation and neovascularization, processes that are governed by fibroblasts and endothelial cells, respectively (Singer and Clark, 1999).

Accumulating evidence indicates an association of high glucose levels with aberrant inflammatory response and poor vascular regeneration (Falanga, 2005a). This association accounts for the high frequency of impaired wound healing in patients with diabetes. The impairment is accompanied by an aberrant inflammatory cell infiltration in the early phase, with the persistence of neutrophils and macrophages in chronic, nonhealing wounds (Falanga, 2005a; Fang et al., 2010; Ochoa et al., 2007b; Wood et al., 2014). Moreover, wounds of genetically diabetic (*db/db*) mice retain a large number of neutrophils and macrophages, with sustained expression of proinflammatory cytokines IL-1β and tumor necrosis factor-α, and chemokines CXCL8 and CCL2, which are potent chemotactic agents for neutrophils and macrophages, respectively (Wetzler et al., 2000). Thus, aberrant chemokine expression can lead to dysregulated inflammatory cell infiltration. Moreover, chemokines can regulate the recruitment and functions of many different cell types including endothelial cells, fibroblasts, and keratinocytes, which are involved in wound repair processes. Thus, the dysregulated chemokine system in diabetic wound sites (Fang et al., 2010; Nishimura et al., 2012; Ochoa et al., 2007b; Wood et al., 2014;) can affect various aspects of diabetic wound healing.

Macrophages can promote the healing process by clearing cellular debris, destroying invading pathogens, and producing a multitude of cytokines, chemokines, and growth factors, which can contribute to neovascularization, an essential process for wound healing (Shaw and Martin, 2009).

[1]Department of Forensic Medicine, Wakayama Medical University, Kimiidera, Wakayama, Japan; [2]Clinical Laboratory Medicine, Wakayama Medical University, Kimiidera, Wakayama, Japan; [3]Cardiovascular Medicine, Wakayama Medical University, Kimiidera, Wakayama, Japan; and [4]Division of Molecular Bioregulation, Cancer Research Institute, Kanazawa University, Kakuma-machi, Kanazawa, Japan

Correspondence: Toshikazu Kondo, Department of Forensic Medicine, Wakayama Medical University, 811-1 Kimiidera, Wakayama 641-8509, Japan. E-mail: kondot@wakayama-med.ac.jp

Abbreviations: BM, bone marrow; EPC, endothelial progenitor cell; STZ, streptozotocin; TGF-β1, transforming growth factor-β1; VEGF, vascular endothelial growth factor

Received 10 October 2018; revised 30 May 2019; accepted 31 May 2019; accepted manuscript published online 24 June 2019; corrected proof published online 6 September 2019

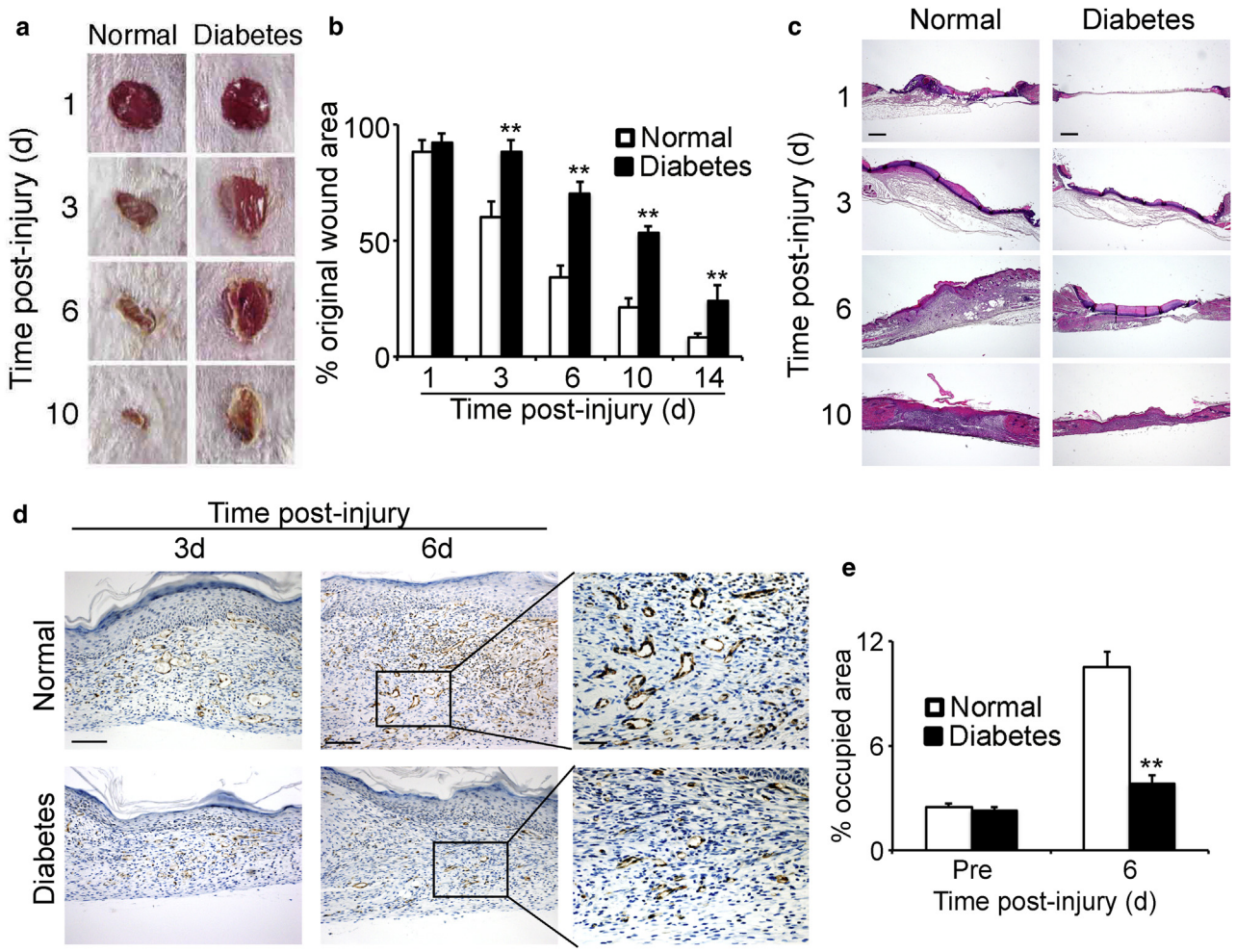


**Figure 1. Delayed wound healing in mice with STZ-induced diabetes.** (**a**) Kinetic analysis of skin excisional wound healing. Representative results from three independent experiments with four animals per group are shown. (**b**) Changes in percentage of wound area at each time point compared with the original wound area are shown. All values represent mean ± SEM. **, $P < 0.01$, versus normal mice. (**c**) Morphological changes in the wounds of normal mice and mice with diabetes. Representative results from six individual animals are shown. Scale bars = 400 μm. (**d**) Immunohistochemical analysis with anti-CD31 mAb 3 and 6 days after the injury. Representative results from six individual animals are shown. Scale bars = 200 μm. Scale bars in inserts = 40 μm. (**e**) The vascular areas were identified as $CD31^+$ areas in wound beds with Adobe Photoshop. All values represent mean ± SEM. **, $P < 0.01$, versus normal mice. SEM, standard error of the mean; STZ, streptozotocin.

Neovascularization can be further promoted by another bone marrow (BM)—derived cell type, endothelial progenitor cells (EPCs). In response to different stimuli such as tissue ischemia, physical exercise, and growth factors, EPCs are mobilized from the BM into the peripheral blood and subsequently migrate to the damaged endothelium in an attempt to restore its integrity, thereby contributing to endothelial and cardiovascular homeostasis (Asahara et al., 1999a). Hence, we investigated the changes in intra-wound macrophages and EPCs in the wound healing process in mice with streptozotocin (STZ)-induced diabetes. Infiltration of both types of cells was depressed at the wound sites of mice with diabetes, together with the depressed expression of a chemokine, CCL2. Moreover, CCL2 administration induced recruitment of both macrophages and EPCs into the wound sites of mice with STZ-induced diabetes and subsequently accelerated wound repair along with markedly increased expression of growth factors such as vascular endothelial growth factor (VEGF) and transforming growth factor-β1 (TGF-β1). Thus, CCL2 therapy could be an attractive strategy for promoting neovascularization and subsequent tissue repair in diabetic wound sites.

## RESULTS

### Delayed wound healing in mice with STZ-induced diabetes

Excisional skin wounds were made to evaluate the effects of diabetes on skin wound healing in vehicle- or STZ-treated mice. In vehicle-treated mice without diabetes, the wound areas were reduced to <40% of the original wound size at 6 days after injury, with complete wound closure at 14 days after the injury (Figure 1a and b). On the other hand, in mice with diabetes, the wound areas still remained 55% of the original injured areas at 10 days after the injury, and the closure had not been completed until 14 days after the injury (Figure 1a and b). Moreover, morphological abnormalities were profound with impaired reepithelialization and granulation tissue formation in mice with diabetes compared with normoglycemic mice until 14 days after the injury

(Figure 1c). Thus, diabetic mice exhibited delayed wound healing, consistent with previous reports (Cianfarani et al., 2006; Graiani et al., 2004; Luo et al., 2004; Sivan-Loukianova et al., 2003; Yue et al., 1987). Neovascularization, a critical step for wound healing, was consistently depressed in the wound sites of mice with diabetes when compared with normoglycemic mice, as revealed by $CD31^+$ areas (Figure 1d and e). Thus, hyperglycemic conditions can impair skin wound healing by depressing neovascularization, a critical step for wound healing.

### Impaired EPC and macrophage recruitment with reduced VEGF and TGF-β expression in mice with diabetes

Accumulating evidence suggests that neovascularization can be promoted in collaboration with several types of hematopoietic-derived cell types, including EPCs and macrophages (Asahara et al., 1999a; Minutti et al., 2017; Motegi and Ishikawa, 2017). Hence, we next assessed EPCs and macrophages in both normal mice and mice with diabetes. We could not detect any differences between normal mice and mice with diabetes in terms of $Tie2^+$ $c\text{-}Kit^+$ EPC numbers in peripheral blood and BM until 4 days after the injury (Supplementary Figure S1). Thus, it is unlikely that diabetic conditions can have an impact on EPC generation in the BM. In contrast, EPC numbers in skin wound sites were reduced in mice with diabetes, compared with those in normoglycemic mice (Figure 2a and b). $F4/80^+$ macrophages started to increase in skin wound sites in normoglycemic mice after 3 days post-injury, whereas the increase was delayed in mice with diabetes (Figure 2c–e). On the contrary, $Gr\text{-}1^+$ granulocyte numbers in skin wound sites of normoglycemic mice reached a maximum 1 day after the injury, decreasing thereafter (Supplementary Figure S2). In contrast, in mice with diabetes neutrophil recruitment was progressively increased until 10 days post-injury, indicating the prolongation of the inflammatory stage (Supplementary Figure S2). There was no difference in T-cell recruitment between normoglycemic mice and mice with diabetes (Supplementary Figure S3). The gene and protein expression of an essential angiogenic factor, VEGF, in skin wound sites was also diminished at the early phase of the healing process (from 3 to 6 days after the injury) in mice with diabetes, compared with normoglycemic mice (Figure 2f and g). Given that macrophages are an important source of VEGF in wounds (Okonkwo and DiPietro, 2017; Singer and Clark, 1999; Werner and Grose, 2003), reduced macrophage infiltration could be linked to the decrease in angiogenesis in diabetic wounds. Consistent with this assumption, a double-color immunofluorescence analysis identified a major cellular source of VEGF in skin wound sites as $F4/80^+$ macrophages (Figure 2h). In addition, $F4/80^+$ macrophages expressed a potent fibrogenic molecule, TGF-β1, as evidenced by a double-color immunofluorescence analysis (Figure 2i). Furthermore, TGF-β1 expression was diminished at both mRNA and protein levels in mice with diabetes, compared with normoglycemic ones (Figure 2j and k). These observations indicate that hyperglycemia can dampen the infiltration of macrophages, which have the capacity to express VEGF and TGF-β1, and additionally suppress the recruitment of EPCs, which are presumed to be crucially involved in neovascularization.

### Depressed CCL2 expression in the diabetic wound healing process

A double-color immunofluorescence analysis further revealed that a specific receptor for CCL2, CCR2, was expressed by $F4/80^+$ cells and $CD31^+$ cells (Figure 3a and b), and to a lesser extent α-smooth muscle actin–positive cells (Supplementary Figure S4), in skin wound sites of normoglycemic mice. These observations prompted us to evaluate the expression of CCL2. *Ccl2* mRNA and its protein expression were enhanced in skin wound sites in normoglycemic mice later than 1 day after the injury, whereas the increments were delayed in mice with diabetes (Figure 3c–e). Moreover, a double-color immunofluorescence analysis demonstrated that CCL2 was expressed mainly by $F4/80^+$ macrophages and α-smooth muscle actin–positive cells (Supplementary Figure S5). These observations would indicate that hyperglycemia-mediated depressed CCL2 expression can suppress the accumulation of CCR2-expressing cells with a capacity to express CCL2, thereby forming a vicious cycle.

### CCL2 treatment reverses wound healing impairment in mice with STZ-induced diabetes

Depressed CCL2 expression in mice with diabetes encouraged us to examine the effects of exogenous CCL2 administration on the wound healing process in these mice. The topical application of CCL2 markedly accelerated wound healing closure rates, reepithelialization, and granulation tissue formation, to a level similar to that observed in normoglycemic mice (Figure 4a–c). CCL2 treatment expanded intra-wound $CD31^+$ vascular areas in mice with diabetes 6 days after the injury (Figure 4d and e). Concomitantly, CCL2 application promoted *Col1a1* mRNA expression and hydroxyproline content, with increased α-smooth muscle actin–positive myofibroblast numbers in mice with diabetes (Figure 4f–h). Although CCL2 promoted the migration of BM-derived cells into skin wound sites (Figure 5a and b), CCL2 selectively increased the intra-wound numbers of EPCs (Figure 5c and d) and macrophages (Figure 5e and f) but not $CD3^+$ T cells (Supplementary Figure S6). Moreover, CCL2-treated mice with diabetes displayed enhanced expression of VEGF and TGF-β1 at the wound sites, compared with phosphate-buffered-saline–treated mice with diabetes (Figure 5g–j). Given that macrophages were a major cellular source of VEGF and TGF-β1 in wound sites, topical CCL2 application could augment neovascularization and collagen accumulation in mice with diabetes, by recruiting EPCs and VEGF- and TGF-β1-expressing macrophages, thereby reversing depressed skin wound healing in mice with diabetes.

### The effects of CCL2 on the expression of VEGF and TGF-β in macrophages

The observation that macrophages were a major cellular source of VEGF and TGF-β1 in wound sites (Figure 2h and i) prompted us to examine in vitro effects of CCL2 on VEGF and TGF-β1 expression in macrophages. CCL2 did enhance *Vegf* and *Tgfb1* mRNA expression in macrophages under high glucose conditions, as well as under normal conditions (Figure 6a and b). Thus, CCL2 can recruit macrophages, a major cellular source of VEGF and TGF-β1, and can simultaneously enhance VEGF and TGF-β1 expression in the

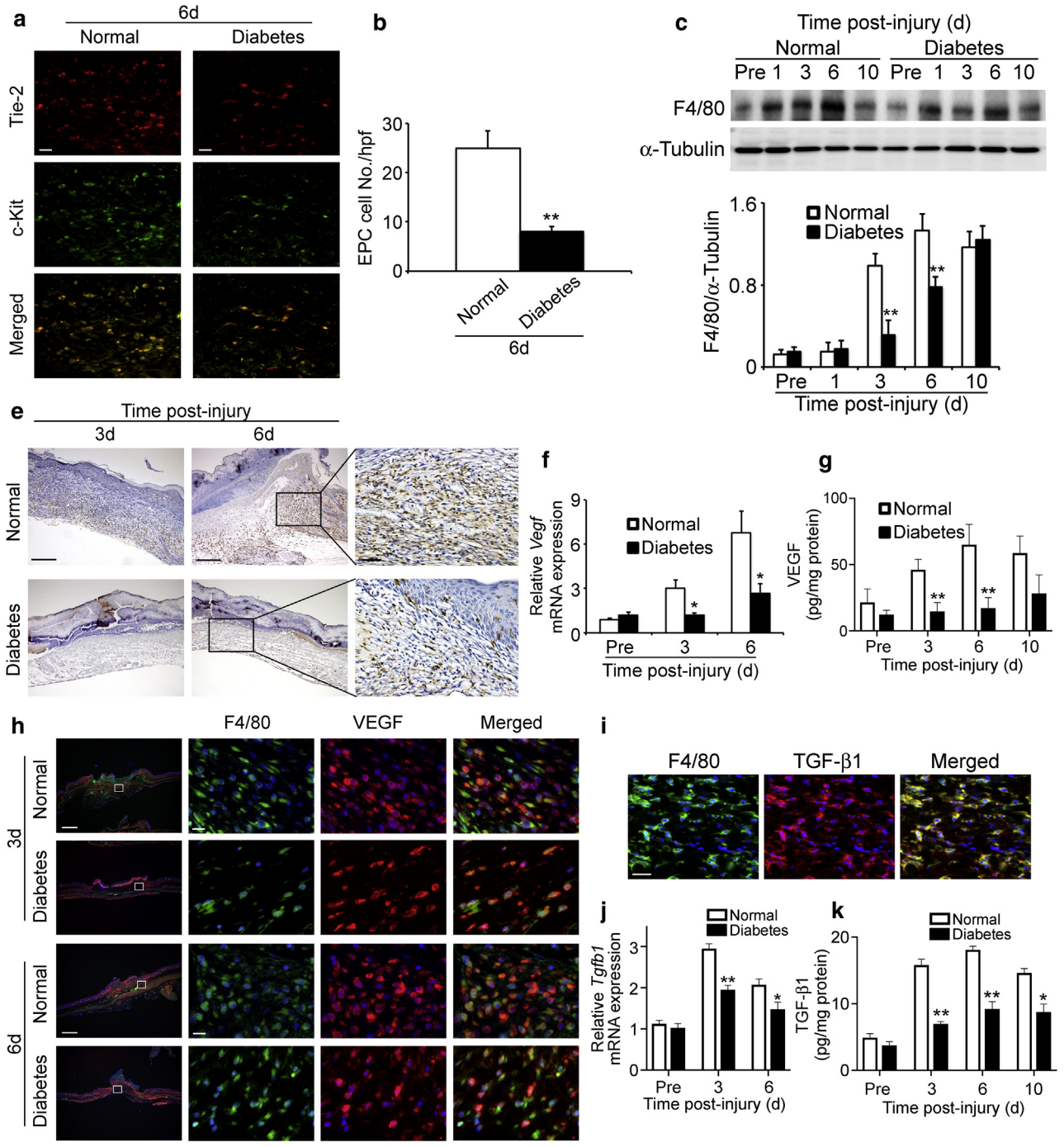


**Figure 2. Impaired EPC and macrophage recruitment in mice with diabetes.** (**a**) A double-color immunofluorescence analysis of Tie2$^+$ c-Kit$^+$ EPCs in wound sites at 6 days after injury in normal mice and mice with diabetes. Representative results from six individual animals are shown. Scale bars = 20 μm. (**b**) Number of Tie2$^+$ c-Kit$^+$ EPCs per high-power microscopic field (original magnification ×400). (**c**) Mice were killed 1, 3, 6, and 10 days after wounding to collect the injured skin areas by using 8 mm diameter biopsy punches. Western blotting analysis was carried out using anti-F4/80 and anti-α-Tubulin mAbs. Representative results from four independent experiments are shown. (**d**) Ratio of F4/80 to α-Tubulin. All values represent mean ± SEM. **, $P < 0.01$, versus normal mice. (**e**) Immunohistochemical detection of F4/80$^+$ macrophages at wound sites in normal mice or mice with diabetes 3 and 6 days after the injury. Representative results from 6 independent experiments are shown. Scale bars = 200 μm. Scale bars in inserts = 40 μm. (**f**) The ratios of *Vegf* to *Actb* at the wound sites were calculated. All values represent mean ± SEM. *, $P < 0.05$, versus normal mice. (**g**) The concentration of VEGF in the wounds of normal mice and mice with diabetes. All values represent mean ± SEM. **, $P < 0.01$ versus normal mice. (**h**) Cell types expressing VEGF. Representative results from six independent experiments are shown (day 3 and 6). Signals merged digitally. Scale bars = 400 μm. Scale bars in inserts = 20 μm. (**i**) Cell types expressing TGF-β1. Representative results from six independent experiments are shown (day 6). Signals merged digitally. Scale bars = 40 μm. (**j**) The ratios of *Tgfb1* to *Actb* at the wound sites were calculated. All values represent mean ± SEM. **, $P < 0.01$; *, $P < 0.05$, versus normal mice. (**k**) The concentration of TGF-β1 in the wound of normal mice and mice with diabetes. All values represent mean ± SEM. **, $P < 0.01$; *, $P < 0.05$, versus normal mice. EPC, endothelial progenitor cell; SEM, standard error of the mean; TGF-β1, transforming growth factor-β1 VEGF, vascular endothelial growth factor.

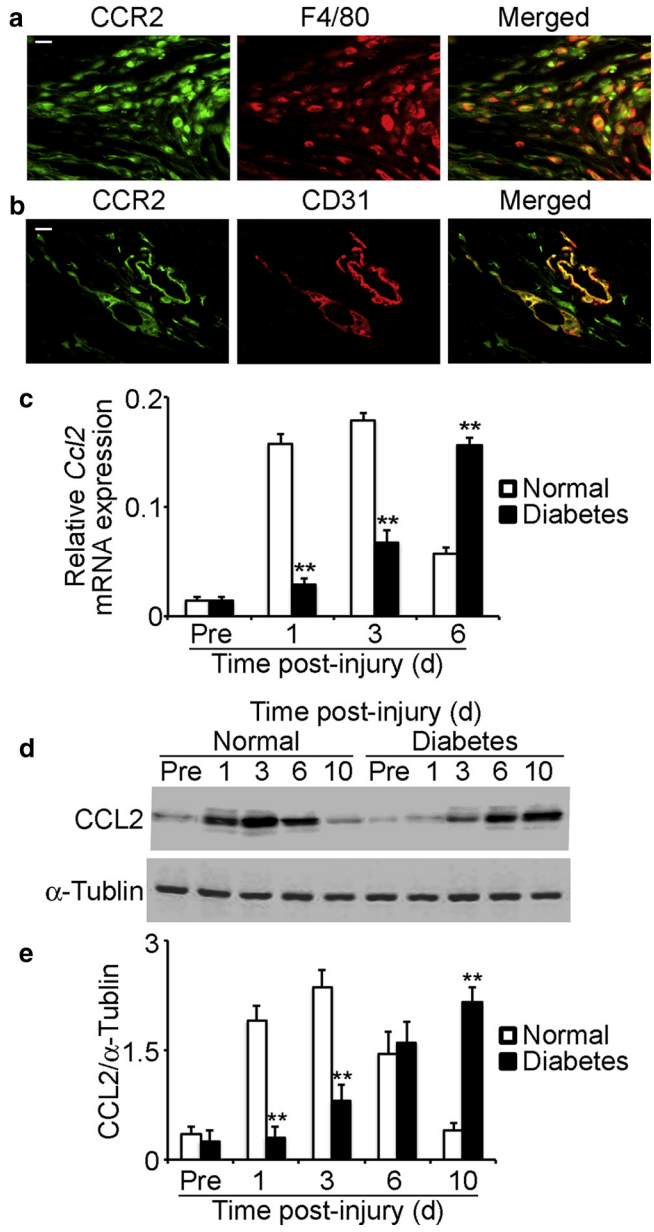


**Figure 3. The kinetics of the CCL2-CCR2 axis expression at skin wound sites.** (**a**, **b**) A double-color immunofluorescence analysis of CCR2-expressing cells in wound sites at 6 days after injury in normal mice. The analysis was performed using (a) anti-CCR2 and anti-F4/80 or (b) anti-CD31, followed by observation under a fluorescence microscope, and signals were merged digitally. Representative results from six individual animals are shown. Scale bars = 20 μm. (**c**) The ratios of *Ccl2* to *Actb* at the wound sites were calculated. (**d**) Western blot analysis for CCL2 in the wound sites. Mice were killed 1, 3, 6, and 10 days after wounding. Eight-millimeter diameter biopsy punches were used to collect the injured skin area. Western blot analysis using anti-α-Tubulin mAb confirmed that an equal amount of protein was loaded onto each lane. Representative results from four independent experiments with four animals in each group are shown. (**e**) Ratio of CCL2 to α-Tubulin. All values represent mean ± SEM. **, $P < 0.01$, versus normal mice. SEM, standard error of the mean.

recruited macrophages, thereby accelerating skin wound healing in mice with diabetes.

### In vitro migratory response of EPCs to CCL2 and VEGF

CCR2 was expressed on $CD31^+$ endothelial cells as wells as $F4/80^+$ macrophages (Figure 3a and b), and several lines of evidence indicated that EPCs also expressed CCR2 and Flk-1, a receptor of VEGF (Ishida et al., 2012; Spring et al., 2005). Hence, we examined the chemotactic activity of CCL2 and VEGF for EPCs. By culturing BM mononuclear cells according to the previously reported method (Asahara et al., 1999b; Ishida et al., 2012), we obtained spindle-shaped EPCs with *Bandeiraea simplicifolia* lectin I-binding and Dil-acetylated low-density lipoprotein uptake abilities (Figure 6c). CCL2 and VEGF induced the migration of the resultant EPCs as efficiently as a well-known EPC chemoattractant, GM-CSF (Figure 6d and e), implying that both CCL2 and VEGF were potent EPC chemoattractants.

## DISCUSSION

Diabetes can induce depressed macrophage infiltration and subsequently augment various tissue injuries. Thioglycollate caused depressed macrophage infiltration into the peritoneal cavity in *db/db* mice, when compared with control mice (Maruyama et al., 2007). Similarly, infection with *Listeria monocytogenes* aggravated liver injury in *db/db* mice, together with impaired macrophage infiltration, when compared with control mice (Ikejima et al., 2005). At the later phase, although diabetic skin ulcers are characterized by a sustained increase in inflammatory leukocytes and in particular macrophages (Bjarnsholt et al., 2008; Blakytny and Jude, 2006; Wetzler et al., 2000;), Wood et al. (2014) demonstrated that diabetic wounds at the early phase exhibited a decrease in macrophage infiltration . In agreement with these observations, we demonstrated that mice with STZ-induced diabetes displayed reduced macrophage infiltration with delayed wound healing and that CCL2 administration reversed the reduced macrophage infiltration and eventually the delay in wound healing in mice with diabetes. Thus, in general, macrophages, which are presumed to be crucially involved in the healing process (Goren et al., 2009; Lucas et al., 2010; Maruyama et al., 2007; Mirza et al., 2009; Wood et al., 2014), can also have an important role in the repair of diabetes-associated skin wounds.

Accumulating evidence has implied that the CCL2-CCR2 axis plays essential roles in mediating homing of monocytes/macrophages to inflamed tissue in various tissue repair models (Lu et al., 2011; Ochoa et al., 2007a; Saederup et al., 2010). Moreover, $Ccl2^{-/-}$ mice exhibited delayed skin wound healing together with depressed angiogenesis and suspended wound re-epithelialization (Low et al., 2001), suggesting a crucial role of CCL2 in the neovascularization observed in skin wound healing. Consistent with this, Qian et al. (2011) reported that the blockade of tumor cell–derived CCL2 inhibited $CCR2^+$ macrophage-derived VEGF production, eventually suppressing tumor metastasis via reduced neovascularization. Thus, the CCL2-CCR2 axis can have a crucial role in neovascularization by regulating the infiltration of macrophages. This assumption encouraged us to examine the effects of topical CCL2 application on diabetic skin wound sites with depressed macrophage infiltration and CCL2 expression.

We observed that the administration of topical CCL2 reversed impaired wound healing in mice with diabetes. However, CCL2 deficiency has previously been shown to marginally, and not significantly, reduce macrophage

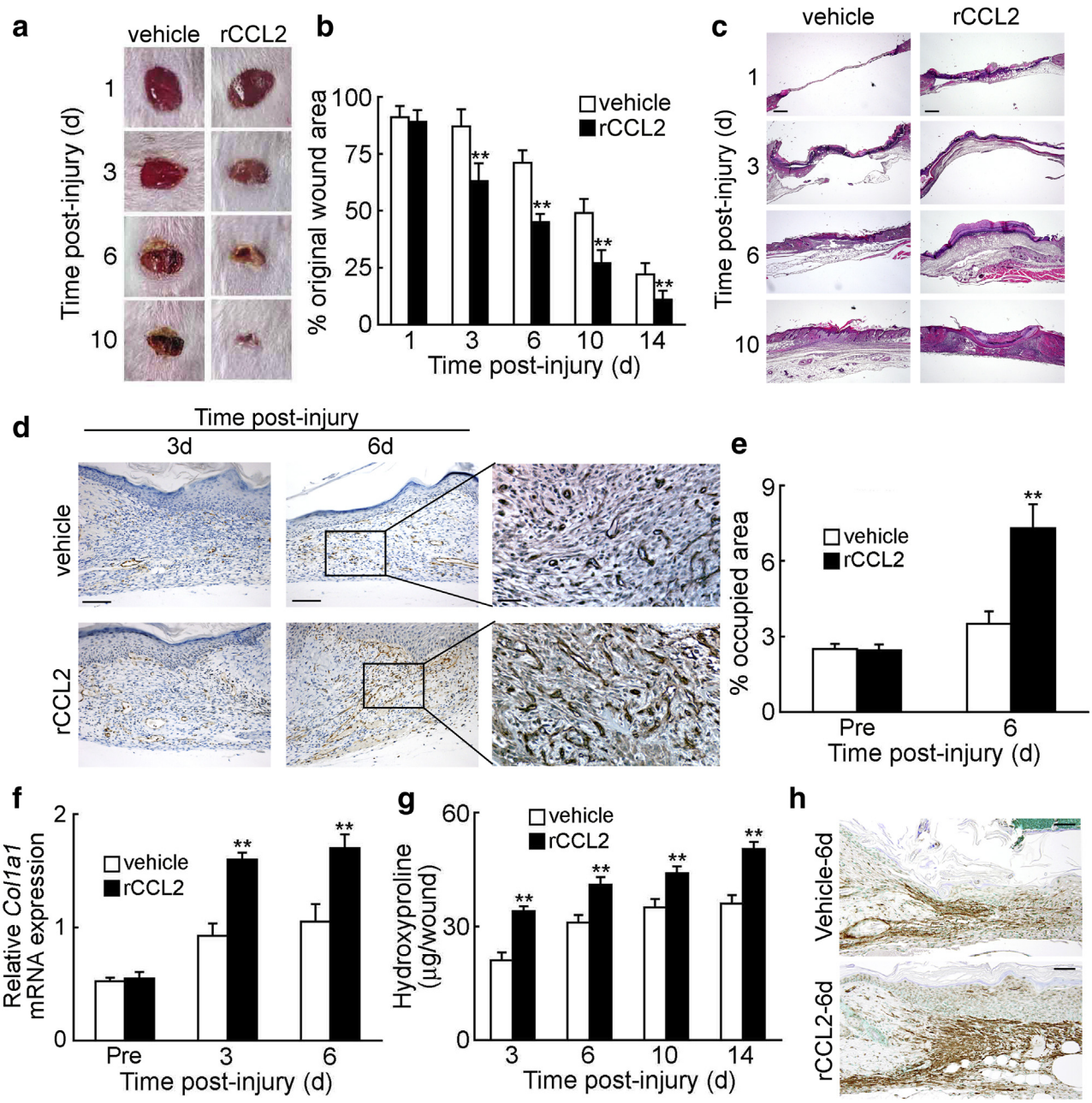


**Figure 4. The reversal of depressed wound healing in mice with diabetes that are treated with CCL2.** (**a**) Macroscopic appearance of wound healing in mice with diabetes administrated with recombinant CCL2 or vehicle alone. The wound sites were photographed at the time indicated. Representative results from 12 individual animals in each group are shown. (**b**) Changes in percentage of wound area at each time point compared with the original wound area. (**c**) Morphological changes in the wounds of mice with diabetes mice treated with CCL2 or the vehicle. Representative results from 6 individual animals are shown. Scale bars = 400 μm. (**d**) Immunohistochemical analysis with anti-CD31 mAb 3 and 6 days after the injury. Representative results from six individual animals are shown. Scale bars = 200 μm. Scale bars in inserts = 40 μm. (**e**) The vascular areas were identified as $CD31^+$ areas in wound beds with Adobe Photoshop. All values represent mean ± SEM. **, $P < 0.01$, versus vehicle-treated mice with diabetes. (**f**) Real-time RT-PCR analysis of *Col1a1* expression at the wound sites. The ratios of *Col1a1* to *Actb* are shown here. All values represent mean ± SEM. **, $P < 0.01$, versus vehicle-treated mice with diabetes. (**g**) Hydroxyproline contents in wound sites. All values represent mean ± SEM. **, $P < 0.01$, versus vehicle-treated mice with diabetes. (**h**) Immunohistochemical analysis of α-SMA, a key marker for myofibroblast differentiation, on wound tissue sections 6 days after injury. Representative results from six individual animals are shown. Scale bars = 100 μm. RT-PCR, reverse transcriptase–PCR; SMA, smooth muscle actin; SEM, standard error of the mean.

infiltration into wound sites (Low et al., 2001), in contrast to our observation that topical CCL2 administration markedly increased macrophage infiltration. These discrepancies may be explained by the different efficacy of endogenous and pharmacological doses of CCL2, in terms of effect on macrophage infiltration. Alternatively, congenital CCL2 deficiency in $Ccl2^{-/-}$ mice may induce compensatory expression of other macrophage-tropic chemokines, which could maintain macrophage infiltration. Nevertheless, angiogenesis has been shown to be markedly impaired in the wound sites of $Ccl2^{-/-}$ mice (Low et al., 2001), similar to that observed in the diabetic wound sites of this study with

reduced CCL2 expression. These observations would indicate an association between reduced CCL2 expression and suppressed angiogenesis in impaired skin wound healing.

Evidence further indicates that macrophages can produce various growth factors such as the potent angiogenic factor VEGF, and the potent fibrogenic factor TGF-β1 (Werner and Grose, 2003). CCL2 could enhance in vitro VEGF and TGF-β1 expression in macrophages, even under hyperglycemic conditions. Consistent with this, the administration of topical CCL2 markedly enhanced intra-wound VEGF and TGF-β1 expression at both gene and protein levels. Thus, CCL2 reversed impaired angiogenesis and collagen accumulation in diabetic skin wound sites, at the very least by inducing the migration of macrophages with a capacity to increase VEGF and TGF-β1 expression in response to CCL2.

BM-derived progenitor cells can contribute to skin wound healing in various organs through the formation of endothelial cells, lymphatic endothelial cells, keratinocytes and myofibroblasts (Falanga, 2009b). In addition, the topical application of BM cells could improve impaired wound healing (Badiavas and Falanga, 2003). Topical application of VEGF to cutaneous wounds reversed the impaired neovascularization observed in *db/db* mice, by mobilizing and recruiting the BM-derived EPCs (Galiano et al., 2004). Gallagher et al. (2007) demonstrated that ischemia induced EPCs in the BM to migrate to hypoxic sites, under the guidance of a concentration gradient of the chemokine CXCL12. The recruited EPCs eventually participated in the formation of new blood vessels. Nishimura et al. (2012) demonstrated that the topical administration of AMD3100, a CXCR4 antagonist, increased EPC counts in peripheral blood and CXCL12 expression at the wound site, leading to improved neovascularization and wound healing. Consistent with this, we previously demonstrated that, once migrated into wound sites, EPCs differentiate into endothelial cells and simultaneously produce growth factors, which further induces the accumulation of endothelial cells and subsequent neovascularization, thereby accelerating wound healing (Ishida et al., 2012). These observations indicate the crucial contribution of EPCs to wound healing.

In human and animal models, diabetes is associated with a decrease in EPCs in circulation and at wound sites, together with decreased CXCL12 expression (Chen et al., 2007; Gallagher et al., 2007; Tepper et al., 2002; Schatteman and Ma, 2006). The administration of human EPCs or CXCL12 reversed impaired EPC recruitment into wound sites and eventually impaired wound healing in genetically diabetic mice (Galiano et al., 2004) and mice with STZ-induced diabetes (Yue et al., 1987). Asai et al. (2006a, 2006b) reported that dibutyryl cAMP and topical Sonic hedgehog gene therapy could accelerate wound healing and promote angiogenesis by enhancing incorporation of EPCs into wounds, in *db/db* mice. Moreover, the same group demonstrated that topical application of EPCs accelerated wound repair and angiogenesis in a murine model of diabetes, in part by providing a source of the growth factors VEGF and basic fibroblast growth factor (Asai et al., 2013). Thus, enhanced EPC migration into wound sites can reverse impaired wound healing in mice with diabetes.

EPCs can express several chemokine receptors, including CCR2 (Ishida et al., 2012; Walenta et al., 2011), and we observed depressed expression of CCL2, a ligand for CCR2, in wound sites of mice with STZ-induced diabetes. These observations encouraged us to evaluate the effects of CCL2 administration on EPC dynamics in wound sites. We provided strong evidence to suggest that CCL2 enhanced EPC migration into wound sites, with few effects on EPC numbers in the BM and peripheral blood. Thus, the administration of CCL2 can promote neovascularization by affecting the migration of EPCs, as well as macrophages, which have crucial impacts on neovascularization. This was further supported by the observation that EPCs induced to migrate by the CCL2-CCR2 axis could contribute to neovascularization, an indispensable event sustaining newly formed granulation tissue (Kado et al., 2018; Spring et al., 2005). Moreover, VEGF also induced in vitro EPC migration as CCL2 did. Thus, the administration of CCL2 promoted EPC recruitment directly through CCR2, and indirectly by inducing VEGF expression in macrophages, and ultimately enhanced neovascularization.

In conclusion, topical application of CCL2 can promote neovascularization, collagen accumulation, and eventual cutaneous wound healing in mice with diabetes. These effects can be mediated by its action on macrophages and EPCs, cells that are crucially involved in angiogenesis and collagen production, essential steps for the wound healing process. Thus, topical CCL2 administration can supplement the therapy for otherwise intractable diabetic skin wounds.

## MATERIALS AND METHODS

### Antibodies

Antibodies used in this study are described in the Supplementary Materials and Methods.

### Animals

*Balb/c* mice were obtained from Clea Japan (Tokyo, Japan) and diabetes was induced by STZ (Sigma-Aldrich, Saint Louis, MO) as described in the Supplementary Materials and Methods. All the mice used for the experiments complied with the standards set out in the Guidelines for the Care and Use of Laboratory Animals at Wakayama Medical University.

### Excisional wound preparation and macroscopic examination

Excisional skin wounds were made in the dorsal skin and obtained as described in the Supplementary Materials and Methods (Ishida et al., 2004, 2006, 2008a, 2012).

### Recombinant CCL2 treatment of wounds

Recombinant CCL2 (R&D Systems, Minneapolis, MN) was injected into each wound bed immediately after wounding as described in the Supplementary Materials and Methods (Dipietro et al., 2001).

### Treatment with PKH26-labeled BM cells in mice

Diabetic recipient mice intravenously received $5 \times 10^6$ PKH26-labeled BM cells in a volume of 200 μl sterile phosphate buffered saline under anesthesia to delineate the trafficking of BM-derived cells, as described in the Supplementary Materials and Methods.

### Quantitative reverse transcriptase–PCR analysis

Quantitative reverse transcriptase–PCR analysis was undertaken as described in the Supplementary Materials and Methods (Ishida et al., 2012).

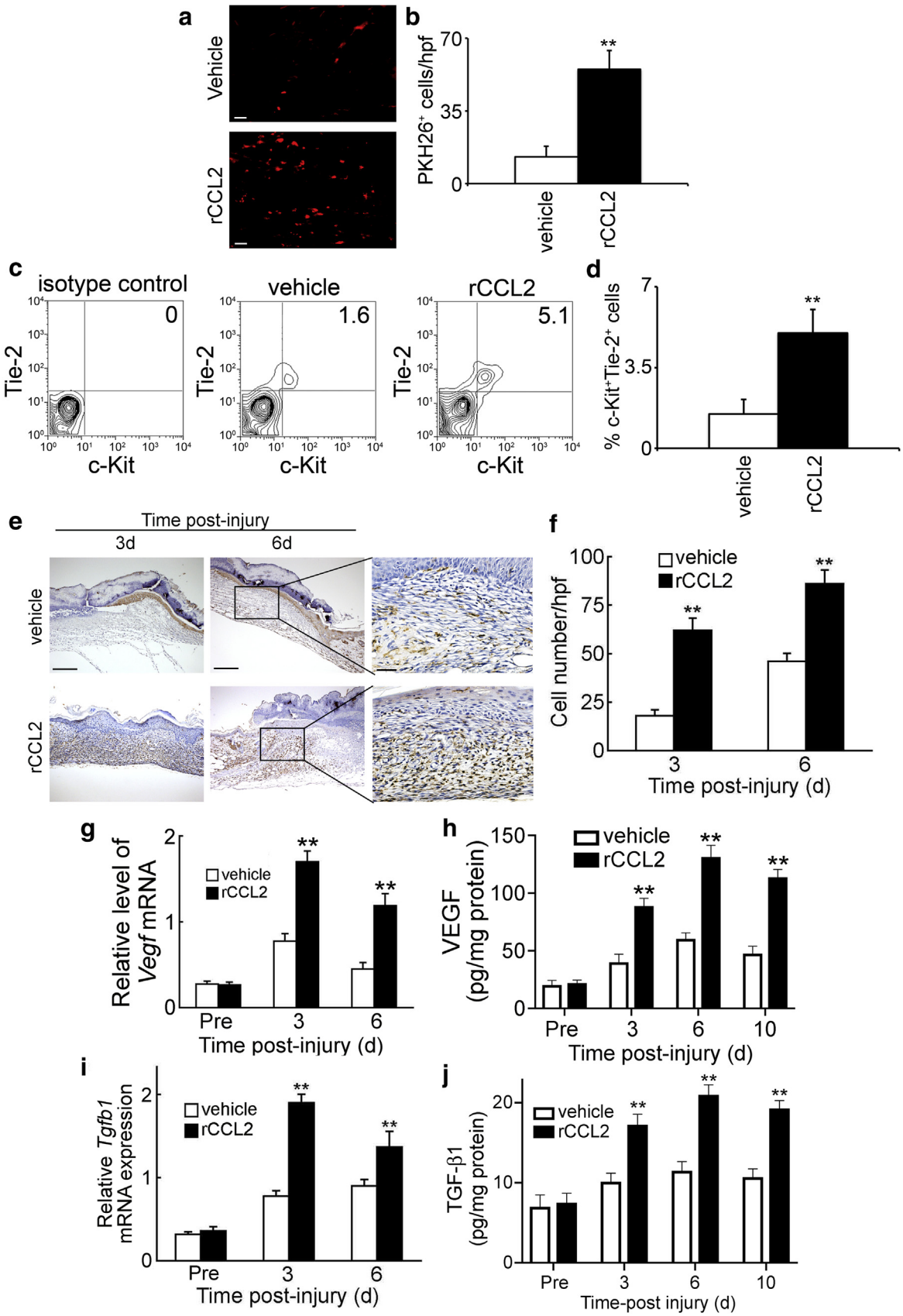


**Figure 5. CCL2 promotes the migration of EPCs and macrophages into skin wounds.** (**a**) BM cells from diabetic donor mice were labeled with the fluorescent dye PKH26. Labeled cells were injected into the tail vein of diabetic recipient mice. Four weeks later, excisional wounds were generated accompanied by topical administration of CCL2. Six days after the injury, wound sites were removed. The migration of PKH26-labeled BM cells to the wound sites was assessed by fluorescent microscopic examination of thin frozen sections. Representative results from six individual animals are shown. Scale bars = 50 μm. (**b**) The

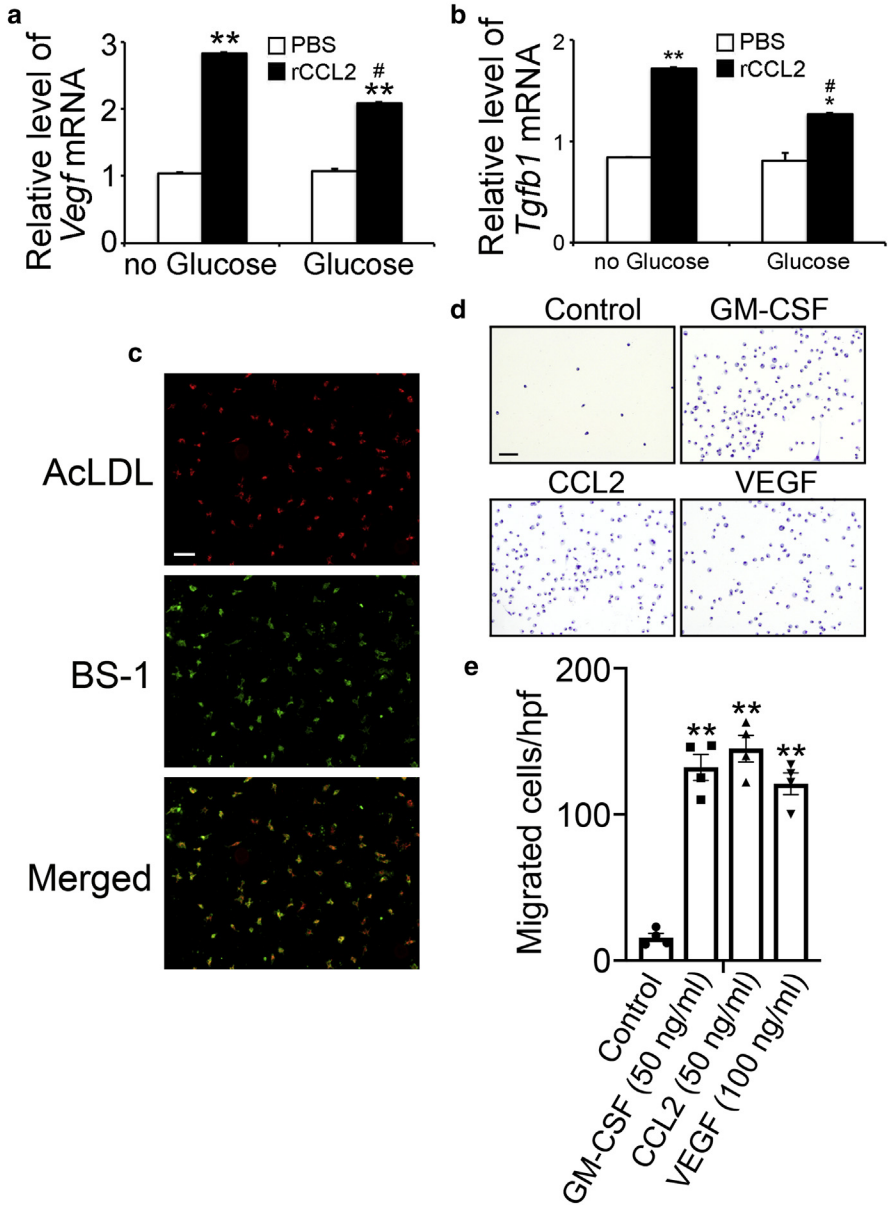


**Figure 6. The effects of CCL2 on the expression of VEGF and TGF-β in macrophages.** (**a**, **b**) Peritoneal macrophages were incubated in the presence or the absence of glucose (30 mM) together with recombinant CCL2 (50 ng/ml) or PBS for 24 hours. Real-time RT-PCR was performed on macrophages treated with CCL2. The ratios of (a) *Vegf* and (b) *Tgfb1* to *Actb* were calculated. All values represent mean ± SEM. **, $P < 0.01$, *, $P < 0.05$ versus PBS; *, $P < 0.05$, versus no-glucose with recombinant CCL2. (**c**) Four days after the initiation of in vitro culture, the resultant EPCs were characterized with both AcLDL uptake (Dil) and *Bandeiraea simplicifolia* lectin I binding (FITC). Scale bar = 100 μm. (**d**, **e**) The effects of CCL2 and VEGF on EPC migration. (d) The cells that migrated into the lower chamber were stained with Giemsa (scale bar = 100 μm), and (e) were counted manually in five random high-power fields (×100) in each well. All values represent mean ± SEM from four independent experiments. **, $P < 0.01$, versus medium alone (control). EPC, endothelial progenitor cell; RT-PCR, reverse transcriptase–PCR; SEM, standard error of the mean; TGF-β, transforming growth factor-β; VEGF, vascular endothelial growth factor

### Histopathological analysis of wound sites

Histopathological and immunohistochemical analyses of wound specimens were performed as described in the Supplementary Materials and Methods (Ishida et al., 2012).

### Double-color immunofluorescence analysis

A double-color immunofluorescence analysis was conducted as described in the Supplementary Materials and Methods (Ishida et al., 2012).

number of PKH26-labeled BM cells per hpf (original magnification ×200) were counted. Values represent mean ± SEM. **, $P < 0.01$, versus vehicle-treated mice with diabetes. (**c**) Quantitative evaluation of EPCs after injury by flow cytometric analysis. Mice were killed 6 days after wounding. Eight-millimeter diameter biopsy punches were used to collect the injured skin area. Diabetic wound sites were analyzed to determine c-Kit$^+$Tie2$^+$ EPCs. Representative results from four independent experiments are shown. A number within the upper right panel in each plot denotes the percentage of cells in the double-positive gate. (**d**) Percentage c-Kit$^+$Tie-2$^+$ EPCs. Values represent mean ± SEM. **, $P < 0.01$, versus vehicle-treated mice with diabetes. (**e**) Immunohistochemical detection of F4/80$^+$ macrophages at wound sites in vehicle- or recombinant CCL2–treated mice with diabetes 3 and 6 days after the injury. Representative results from 6 independent experiments are shown. Scale bars = 200 μm. Scale bars in inserts = 40 μm. (**f**) Number of F4/80$^+$ macrophages per hpf (original magnification ×200). All values represent mean ± SEM. **, $P < 0.01$, versus vehicle-treated mice with diabetes. (**g**) Real-time RT-PCR analysis of *Vegf* at the wound sites in CCL2- or vehicle-treated animals. The ratios of *Vegf* to *Actb* were calculated. (**h**) The concentration of VEGF at the wound sites of CCL2- or vehicle-treated mice with diabetes. (**i**) Real-time RT-PCR analysis of *Tgfb1* at the wound sites in CCL2- or vehicle-treated animals. The ratios of *Tgfb1* to *Actb* were calculated. (**j**) The concentration of TGF-β1 at the wound sites of CCL2- or vehicle-treated mice with diabetes. All values represent mean ± SEM. **, $P < 0.01$, versus vehicle-treated mice with diabetes. BM, bone marrow, EPC, endothelial progenitor cell; hpf, high-power field; RT-PCR, reverse transcriptase–PCR; SEM, standard error of the mean; TGF-β1, transforming growth factor-β1; VEGF, vascular endothelial growth factor.

### Measurement of leukocyte and EPC numbers, and neovascularization at wound sites

The number of leukocytes and EPCs and the intensity of neovascularization were evaluated as described in the Supplementary Materials and Methods (Ishida et al., 2012).

### Western blotting analysis

Wound samples were subjected to western blotting analysis as described in the Supplementary Materials and Methods (Ishida et al., 2004a).

### Determination of hydroxyproline content in skin wound sites

Hydroxyproline content was measured as described in the Supplementary Materials and Methods (Ishida et al., 2006).

### Mononuclear cell isolation and flow cytometric analysis

Mononuclear cells were isolated from BM, peripheral blood, and wound tissue homogenates, followed by flow cytometric analysis as described in the Supplementary Materials and Methods (Ishida et al., 2012).

### ELISA for VEGF and TGF-β1 protein levels

Wound tissues were subjected to ELISA for the measurement of VEGF and TGF-β1 protein levels as described in the Supplementary Materials and Methods (Ishida et al., 2004, 2006, 2008a, 2012).

### In vitro culture of peritoneal macrophages

Cells were collected from the peritoneal cavity of thioglycollate-injected mice with diabetes, followed by subsequent analysis as described in the Supplementary Materials and Methods (Ishida et al., 2008b; Maruyama et al., 2007).

### In vitro EPC migration assay

EPCs were isolated followed by a migration assay as described in the Supplementary Materials and Methods (Asahara et al., 1999b; Yoon et al., 2006).

### Statistical analysis

Statistical analyses were performed as described in the Supplementary Materials and Methods.

### Data availability statement

No data sets were generated or analyzed during this study.

## CONFLICT OF INTEREST

The authors state no conflict of interest.

## ACKNOWLEDGEMENTS

This study was financially supported in part by Grants-in-Aids for Scientific Research (TK, MN, and YI) from Japan Society for the Promotion of Science, a Grant-in-Aid for Medical Research (TK) from Mitsui Life Social Welfare Foundation, and The Uehara Memorial Foundation (TK).

## AUTHOR CONTRIBUTIONS

Conceptualization: YI, TK; Formal Analysis: YI, YK; Funding Acquisition: TK, MN, YI; Investigation: MN, AK, MF, MA; Project Administration: TK; Validation: AT, HY, ES; Writing - Original Draft Preparation: YI; Writing - Review and Editing: NM, TK.

## SUPPLEMENTARY MATERIAL

Supplementary material is linked to the online version of the paper at www.jidonline.org, and at https://doi.org/10.1016/j.jid.2019.05.022.

## REFERENCES

Asahara T, Masuda H, Takahashi T, Kalka C, Pastore C, Silver M, et al. Bone marrow origin of endothelial progenitor cells responsible for postnatal vasculogenesis in physiological and pathological neovascularization. Circ Res 1999a;85:221–8.

Asahara T, Takahashi T, Masuda H, Kalka C, Chen D, Iwaguro H, et al. VEGF contributes to postnatal neovascularization by mobilizing bone marrow-derived endothelial progenitor cells. EMBO J 1999b;18:3964–72.

Asai J, Takenaka H, Ii M, Asahi M, Kishimoto S, Katoh N, et al. Topical application of ex vivo expanded endothelial progenitor cells promotes vascularisation and wound healing in diabetic mice. Int Wound J 2013;10:527–33.

Asai J, Takenaka H, Katoh N, Kishimoto S. Dibutyryl cAMP influences endothelial progenitor cell recruitment during wound neovascularization. J Invest Dermatol 2006a;126:1159–67.

Asai J, Takenaka H, Kusano KF, Ii M, Luedemann C, Curry C, et al. Topical sonic hedgehog gene therapy accelerates wound healing in diabetes by enhancing endothelial progenitor cell-mediated microvascular remodeling. Circulation 2006b;113:2413–24.

Badiavas EV, Falanga V. Treatment of chronic wounds with bone marrow-derived cells. Arch Dermatol 2003;139:510–6.

Bjarnsholt T, Kirketerp-Møller K, Jensen PØ, Madsen KG, Phipps R, Krogfelt K, et al. Why chronic wounds will not heal: a novel hypothesis. Wound Repair Regen 2008;16:2–10.

Blakytny R, Jude E. The molecular biology of chronic wounds and delayed healing in diabetes. Diabet Med 2006;23:594–608.

Chen YH, Lin SJ, Lin FY, Wu TC, Tsao CR, Huang PH, et al. High glucose impairs early and late endothelial progenitor cells by modifying nitric oxide-related but not oxidative stress-mediated mechanisms. Diabetes 2007;56:1559–68.

Cianfarani F, Zambruno G, Brogelli L, Sera F, Lacal PM, Pesce M, et al. Placenta growth factor in diabetic wound healing: altered expression and therapeutic potential. Am J Pathol 2006;169:1167–82.

Dipietro LA, Reintjes MG, Low QE, Levi B, Gamelli RL. Modulation of macrophage recruitment into wounds by monocyte chemoattractant protein-1. Wound Repair Regen 2001;9:28–33.

Falanga V. Wound healing and its impairment in the diabetic foot. Lancet 2005;366:1736–43.

Falanga V. Bone marrow cells can manipulate healing. Blood 2009;113:982–3.

Fang Y, Shen J, Yao M, Beagley KW, Hambly BD, Bao S. Granulocyte-macrophage colony-stimulating factor enhances wound healing in diabetes via upregulation of proinflammatory cytokines. Br J Dermatol 2010;162:478–86.

Galiano RD, Tepper OM, Pelo CR, Bhatt KA, Callaghan M, Bastidas N, et al. Topical vascular endothelial growth factor accelerates diabetic wound healing through increased angiogenesis and by mobilizing and recruiting bone marrow-derived cells. Am J Pathol 2004;164:1935–47.

Gallagher KA, Liu ZJ, Xiao M, Chen H, Goldstein LJ, Buerk DG, et al. Diabetic impairments in NO-mediated endothelial progenitor cell mobilization and homing are reversed by hyperoxia and SDF-1 alpha. J Clin Invest 2007;117:1249–59.

Goren I, Allmann N, Yogev N, Schürmann C, Linke A, Holdener M, et al. A transgenic mouse model of inducible macrophage depletion: effects of diphtheria toxin-driven lysozyme M-specific cell lineage ablation on wound inflammatory, angiogenic, and contractive processes. Am J Pathol 2009;175:132–47.

Graiani G, Emanueli C, Desortes E, Van Linthout S, Pinna A, Figueroa CD, et al. Nerve growth factor promotes reparative angiogenesis and inhibits endothelial apoptosis in cutaneous wounds of type 1 diabetic mice. Diabetologia 2004;47:1047–54.

Ikejima S, Sasaki S, Sashinami H, Mori F, Ogawa Y, Nakamura T, et al. Impairment of host resistance to Listeria monocytogenes infection in liver of db/db and ob/ob mice. Diabetes 2005;54:182–9.

Ishida Y, Gao JL, Murphy PM. Chemokine receptor CX3CR1 mediates skin wound healing by promoting macrophage and fibroblast accumulation and function. J Immunol 2008a;180:569–79.

Ishida Y, Hayashi T, Goto T, Kimura A, Akimoto S, Mukaida N, et al. Essential involvement of CX3CR1-mediated signals in the bactericidal host defense during septic peritonitis. J Immunol 2008b;181:4208–18.

Ishida Y, Kimura A, Kuninaka Y, Inui M, Matsushima K, Mukaida N, et al. Pivotal role of the CCL5/CCR5 interaction for recruitment of endothelial progenitor cells in mouse wound healing. J Clin Invest 2012;122:711–21.

Ishida Y, Kondo T, Kimura A, Matsushima K, Mukaida N. Absence of IL-1 receptor antagonist impaired wound healing along with aberrant NF-κB

activation and a reciprocal suppression of TGF-β signal pathway. J Immunol 2006;176:5598–606.

Ishida Y, Kondo T, Takayasu T, Iwakura Y, Mukaida N. The essential involvement of cross-talk between IFN-γ and TGF-β in the skin wound-healing process. J Immunol 2004;172:1848–55.

Kado M, Tanaka R, Arita K, Okada K, Ito-Hirano R, Fujimura S, et al. Human peripheral blood mononuclear cells enriched in endothelial progenitor cells via quality and quantity controlled culture accelerate vascularization and wound healing in a porcine wound model. Cell Transplant 2018;27:1068–79.

Low QE, Drugea IA, Duffner LA, Quinn DG, Cook DN, Rollins BJ, et al. Wound healing in MIP-1$\alpha^{-/-}$ and MCP-1$^{-/-}$ mice. Am J Pathol 2001;159:457–63.

Lu H, Huang D, Saederup N, Charo IF, Ransohoff RM, Zhou L. Macrophages recruited via CCR2 produce insulin-like growth factor-1 to repair acute skeletal muscle injury. FASEB J 2011;25:358–69.

Lucas T, Waisman A, Ranjan R, Roes J, Krieg T, Müller W, et al. Differential roles of macrophages in diverse phases of skin repair. J Immunol 2010;184:3964–77.

Luo JD, Wang YY, Fu WL, Wu J, Chen AF. Gene therapy of endothelial nitric oxide synthase and manganese superoxide dismutase restores delayed wound healing in type 1 diabetic mice. Circulation 2004;110:2484–93.

Maruyama K, Asai J, Ii M, Thorne T, Losordo DW, D'Amore PA. Decreased macrophage number and activation lead to reduced lymphatic vessel formation and contribute to impaired diabetic wound healing. Am J Pathol 2007;170:1178–91.

Minutti CM, Knipper JA, Allen JE, Zaiss DM. Tissue-specific contribution of macrophages to wound healing. Semin Cell Dev Biol 2017;61:3–11.

Mirza R, DiPietro LA, Koh TJ. Selective and specific macrophage ablation is detrimental to wound healing in mice. Am J Pathol 2009;175:2454–62.

Motegi SI, Ishikawa O. Mesenchymal stem cells: the roles and functions in cutaneous wound healing and tumor growth. J Dermatol Sci 2017;86:83–9.

Nishimura Y, Ii M, Qin G, Hamada H, Asai J, Takenaka H, et al. CXCR4 antagonist AMD3100 accelerates impaired wound healing in diabetic mice. J Invest Dermatol 2012;132:711–20.

Ochoa O, Sun D, Reyes-Reyna SM, Waite LL, Michalek JE, McManus LM, et al. Delayed angiogenesis and VEGF production in CCR2-/- mice during impaired skeletal muscle regeneration. Am J Physiol Regul Integr Comp Physiol 2007a;293:R651–61.

Ochoa O, Torres FM, Shireman PK. Chemokines and diabetic wound healing. Vascular 2007b;15:350–5.

Okonkwo UA, DiPietro LA. Diabetes and wound angiogenesis. Int J Mol Sci 2017;18:E1419.

Qian BZ, Li J, Zhang H, Kitamura T, Zhang J, Campion LR, et al. CCL2 recruits inflammatory monocytes to facilitate breast-tumour metastasis. Nature 2011;475:222–5.

Saederup N, Cardona AE, Croft K, Mizutani M, Cotleur AC, Tsou CL, et al. Selective chemokine receptor usage by central nervous system myeloid cells in CCR2-red fluorescent protein knock-in mice. PLoS One 2010;5:e13693.

Schatteman GC, Ma N. Old bone marrow cells inhibit skin wound vascularization. Stem Cells 2006;24:717–21.

Shaw TJ, Martin P. Wound repair at a glance. J Cell Sci 2009;122:3209–13.

Singer AJ, Clark RA. Cutaneous wound healing. N Engl J Med 1999;341:738–46.

Sivan-Loukianova E, Awad OA, Stepanovic V, Bickenbach J, Schatteman GC. CD34$^{+}$ blood cells accelerate vascularization and healing of diabetic mouse skin wounds. J Vasc Res 2003;40:368–77.

Spring H, Schüler T, Arnold B, Hämmerling GJ, Ganss R. Chemokines direct endothelial progenitors into tumor neovessels. Proc Natl Acad Sci USA 2005;102:18111–6.

Tepper OM, Galiano RD, Capla JM, Kalka C, Gagne PJ, Jacobowitz GR, et al. Human endothelial progenitor cells from type II diabetics exhibit impaired proliferation, adhesion, and incorporation into vascular structures. Circulation 2002;106:2781–6.

Walenta KL, Bettink S, Böhm M, Friedrich EB. Differential chemokine receptor expression regulates functional specialization of endothelial progenitor cell subpopulations. Basic Res Cardiol 2011;106:299–305.

Werner S, Grose R. Regulation of wound healing by growth factors and cytokines. Physiol Rev 2003;83:835–70.

Wetzler C, Kämpfer H, Stallmeyer B, Pfeilschifter J, Frank S. Large and sustained induction of chemokines during impaired wound healing in the genetically diabetic mouse: prolonged persistence of neutrophils and macrophages during the late phase of repair. J Invest Dermatol 2000;115:245–53.

Wood S, Jayaraman V, Huelsmann EJ, Bonish B, Burgad D, Sivaramakrishnan G, et al. Pro-inflammatory chemokine CCL2 (MCP-1) promotes healing in diabetic wounds by restoring the macrophage response. PLoS One 2014;9:e91574.

Yoon CH, Hur J, Oh IY, Park KW, Kim TY, Shin JH, et al. Intercellular adhesion molecule-1 is upregulated in ischemic muscle, which mediates trafficking of endothelial progenitor cells. Arterioscler Thromb Vasc Biol 2006;26:1066–72.

Yue DK, McLennan S, Marsh M, Mai YW, Spaliviero J, Delbridge L, et al. Effects of experimental diabetes, uremia, and malnutrition on wound healing. Diabetes 1987;36:295–9.

## SUPPLEMENTARY MATERIALS AND METHODS

### Antibodies

The following mAbs and polyclonal antibodies (pAbs) were used in this study: hamster anti-mouse CCL2 mAb (LifeSpan BioSciences, Seattle, WA); goat anti-mouse CCR2 pAbs (Santa Cruz Biotechnology, Dallas, TX); rat anti-mouse F4/80 mAb (Bio-Rad Laboratories, Hercules, CA); rat anti-mouse CD31 mAb (BD Biosciences, San Jose, CA); rat anti-mouse Gr-1 mAb (clone 1A8) (BD Biosciences); rabbit anti-mouse Tie2 pAbs (Santa Cruz Biotechnology); goat anti-mouse c-Kit pAbs (R&D Systems, Minneapolis, MN); rabbit anti-human CD3 pAbs (DakoCytomation, Glostrup, Denmark), which cross-reacts with mouse CD3; mouse anti-human α-smooth muscle actin mAb (clone 1A4) (DakoCytomation), which cross-reacts with mouse α-smooth muscle actin; goat anti-mouse transforming growth factor-β1 (TGF-β1) pAbs (Santa Cruz Biotechnology); rat anti-mouse Gr-1 mAb (clone RB6-8C5) (BD Biosciences); mouse anti-mouse α-Tubulin mAb (Santa Cruz Biotechnology); rabbit anti-mouse vascular endothelial growth factor (VEGF) pAbs (Santa Cruz Biotechnology); cyanine dye 3—conjugated donkey anti-rat, -rabbit, -goat, and -mouse immunoglobulin G pAbs (Jackson ImmunoResearch, West Grove, PA); and FITC-conjugated donkey anti-rat, -mouse, -hamster, and -goat immunoglobulin G pAbs (Jackson ImmunoResearch). For flow cytometric analysis, the following mAbs were commercially obtained: FITC-conjugated rat anti-mouse c-Kit mAb (BD Biosciences) and phycoerythrin-conjugated rat anti-mouse Tie2 mAb (Thermo Fisher Scientific, Waltham, MA).

### Animals

Pathogen-free 8- to 10-week-old male *Balb/c* mice were obtained from Clea Japan (Tokyo, Japan). The mice were provided with sterile food and water in an environmentally controlled room. All the mice used for the experiments complied with the standards set out in the Guidelines for the Care and Use of Laboratory Animals at Wakayama Medical University and were housed individually in cages under specific pathogen-free conditions during the whole course of the study. Diabetes was experimentally induced by a single intraperitoneal injection of streptozotocin (Sigma-Aldrich, Saint Louis, MO) at a dose of 200 mg/kg weight in 0.1 M citrate buffer (pH 4.5). Nondiabetic control mice received an equal volume of citrate buffer without streptozotocin. At 7 days after streptozotocin injection, the blood glucose level was measured with a Fuji DRI-CHEM 3500V as instructed by the manufacturer (FUJIFILM Medical Systems, Tokyo, Japan). Only mice with a fasting blood glucose level of >300 mg/dl were considered diabetic and subjected to the following experiments.

### Excisional wound preparation and macroscopic examination

Mice were anesthetized with ketamine-xylazine and full-thickness excisional skin wounds were made in the dorsal skin under sterile conditions. Briefly, after shaving and wiping with 70% ethanol, the dorsal skin was picked up at the midline and punched through two layers of skin with a sterile disposable 4 mm in diameter biopsy punch (Kai Industries, Tokyo, Japan). The same procedure was repeated 3 times, generating a total of 6 wounds on each animal. Each wound site was digitally photographed at the indicated time intervals, and wound areas were determined on photographs using Adobe Photoshop (Adobe, San Jose, CA). Changes in wound areas were expressed as a proportion of the initial wound areas. Subsequently, wounds and their surrounding areas, including the scab and epithelial margins, were cut for further analysis with a sterile disposable biopsy punch with a diameter of 8 mm at the indicated time intervals.

### Recombinant CCL2 treatment of wounds

Recombinant CCL2 was commercially obtained from R&D Systems. In some experiments, 100 ng of CCL2 in 25 μl of vehicle (10 mg collagen/ml phosphate buffered saline [PBS]) or vehicle alone was injected into each wound bed immediately after wounding. Thereafter, animals received a similar injection each day for a period of up to day 2 after wound preparation.

### Treatment with PKH26-labeled bone marrow cells in mice

Bone marrow (BM) cells were collected from the femurs of diabetic donor mice by aspiration and flushing and were labeled with PKH26 (Sigma-Aldrich), a lipophilic red fluorescent dye that stains the membrane of viable cells and is distributed into each mitotic cells, according to the manufacturer's instructions. It has an emission wavelength of 567 nm and a half-life of longer than 100 days. Diabetic recipient mice intravenously received $5 \times 10^6$ PKH26-labeled BM cells in a volume of 200 μl sterile phosphate buffered saline under anesthesia to delineate the trafficking of BM-derived cells. The recipients were fed normal chow and autoclaved hyperchlorinated water for 4 weeks. Then, full-thickness skin wounds were made and treated with CCL2 in the recipients as described above. PKH26-labeled cells were visualized in frozen sections of skin wounds using fluorescence microscopy and the appropriate filter.

### Quantitative reverse transcriptase—PCR analysis

Total RNA was extracted from injured and uninjured skin samples using ISOGEN (NIPPON GENE, Toyama, Japan), according to the manufacturer's instructions. Total RNA was reverse transcribed to cDNA using PrimeScript Reverse Transcriptase (Takara Bio, Shiga, Japan) with oligo(deoxythymine)$_{15}$ primers. Real-time PCR was carried out using SYBR Premix Ex Taq II (Takara Bio) with specific primer sets (Supplementary Table 1). Amplification and detection of the amplified products were performed using the TP800 Thermal Cycler Dice Real Time System (Takara Bio) according to the manufacturer's instructions. To standardize mRNA levels, transcript levels of *Actb* were determined in parallel for each sample, and relative transcript levels were corrected by normalization based on *Actb* transcript levels.

### Histopathological analysis of wound sites

Wound specimens were fixed in 4% formaldehyde buffered with PBS and then embedded with paraffin. Sections were stained with hematoxylin and eosin for histological analysis. Immunohistochemical analysis was also performed using anti-Gr-1, -F4/80, -CD31, -CD3, or -α-smooth muscle actin antibodies (Abs). Deparaffinized sections were immersed in 0.3% hydrogen peroxide in methanol for 30 minutes to eliminate endogenous peroxidase activities. The sections were further incubated with PBS containing 1% normal serum corresponding to the secondary Abs and 1% BSA to

reduce nonspecific reactions. The sections were incubated with Abs at a concentration of 1 μg/ml at 4°C overnight. Normal rat, rabbit, goat, or mouse immunoglobulin G was used as a negative control. After incubation with biotinylated secondary Abs, immune complexes were visualized using the Catalyzed Signal Amplification System (DakoCytomation) according to the manufacturer's instructions.

**Double-color immunofluorescence analysis**

A double-color immunofluorescence analysis was conducted to identify the types of cells expressing CCR2, CCL2, VEGF, and TGF-β1, and $Tie2^+$ $c\text{-}Kit^+$ endothelial progenitor cells (EPCs) in the wounds. Thereafter, the sections were observed under a fluorescence microscope.

**Measurement of leukocyte and EPC numbers, and neovascularization at wound sites**

The wound bed was defined as the area surrounded by uninjured skin and fascia, regenerated epidermis, and eschar. The numbers of infiltrating $F4/80^+$ macrophages, $CD3^+$ T cells, and $Tie2^+$ $c\text{-}Kit^+$ EPCs within the wound beds were enumerated on 5 randomly chosen visual fields ($F4/80^+$ macrophages and $CD3^+$ T cells, magnification ×200; $Tie2^+$ $c\text{-}Kit^+$ EPCs, magnification ×400) of the sections, and the average of the selected 5 fields was calculated. Using the freehand tool of Adobe Photoshop, vascular areas, defined as CD31-immunoreactive areas in the wound beds, were measured and were expressed as the percentage of the entire wound bed area. All measurements were performed by two individual observers without prior knowledges on experimental procedures.

**Western blotting analysis**

The wounds and their surrounding areas, including the scab and epithelial margins, were cut with a sterile disposable biopsy punch with a diameter of 8 mm at the indicated time intervals. Wound samples were homogenized and the resultant lysates (30 μg) were electrophoresed in a 7.5% SDS-PAGE gel and transferred onto a nitrocellulose membrane. The membrane was then incubated with Abs to F4/80, CCL2, or Gr-1, diluted 1,000-fold. After the incubation of horseradish peroxidase—conjugated secondary Abs, the immune complexes were visualized using an ECL Plus System (Amersham Biosciences, Piscataway, NJ) according to the manufacturer's instructions.

**Determination of hydroxyproline content in skin wound sites**

At the indicated time intervals after the injury, skin wound samples were obtained using a sterile disposable biopsy punch as described above. Thereafter, hydroxyproline content was measured as an index of collagen accumulation at the wound sites. Hydroxyproline content was calculated by comparison to standards (Sigma-Aldrich) and expressed as the amount per wound in micrograms.

**Mononuclear cell isolation and flow cytometric analysis**

Mononuclear cells were isolated from BM, peripheral blood, and wound tissue homogenates. Contaminated red blood cells were removed using ammonium chloride solution (Imgenex, San Diego, CA). The resulting single cell suspensions were incubated with a combination of phycoerythrin-conjugated rat anti-mouse Tie2 and FITC-conjugated rat anti-mouse c-Kit mAbs for 20 minutes on ice. Isotype-matched control immunoglobulins were used to detect nonspecific binding of immunoglobulin. The stained cells were analyzed on a BD FACSCalibur flow cytometer (BD Biosciences), and the obtained data were analyzed using BD CellQuest Pro software (BD Biosciences). $Tie2^+$ $c\text{-}Kit^+$ cells within the myeloid mononuclear cell population were labeled as EPCs.

**ELISA for VEGF and TGF-β1 protein levels**

Wound tissues were obtained and were homogenized with 0.5 ml lysis buffer (10 mM PBS, 0.1% SDS, 1% Nonidet P-40, and 5 mM EDTA) containing Complete Protease Inhibitor Mixture (Roche Diagnostics, Indianapolis, IN). The homogenates were centrifuged at 18,000*g* for 15 minutes. VEGF and TGF-β1 protein levels were measured with commercially available Quantikine ELISA kits (R&D Systems) according to the manufacturer's recommendations. The detection limits for each method were as follows: VEGF > 3 pg/ml; TGF-β1 > 7 pg/ml. The total protein in the supernatant was measured with the commercially available Pierce BCA Protein Assay Kit (Thermo Fisher Scientific). The data were expressed as growth factor (in pg/ml) relative to total protein (in mg/ml) for each sample.

**In vitro culture of peritoneal macrophages**

Cells were collected from the peritoneal cavity of thioglycollate-injected diabetic mice. The resultant cells were cultured for 24 hours at 37 °C in 5% $CO_2$ ($1 \times 10^6$ cells/ml) in complete medium consisting of RPMI1640 medium with 10% BSA and $1 \times 10^{-5}$ M 2-mercaptoethanol, and adherent cells were then harvested as macrophages. The glucose-high medium was prepared by adding glucose to the complete medium to a final concentration of 300 mmol/L. Macrophages were cultured for 24 hours in the presence or the absence of 50 mg/ml CCL2 (BD Biosciences) in the glucose-high medium.

**In vitro EPC migration assay**

Whole BM cells were harvested by flushing femurs and tibias with PBS, and mononuclear cells were isolated by Histopaque-1083 (Sigma-Aldrich) density gradient centrifugation. Isolated BM mononuclear cells were cultured in EBM-2 BulletKit medium (Lonza, Walkersville, MD) supplemented with 5% fetal bovine serum, antibiotics and growth factors (EPC medium) on fibronectin-coated 6-well plates or fibronectin-coated 4-well glass slides (BD Biosciences). Four to 7 days after culture, the resultant attached spindle-shaped cells were confirmed to express the markers of EPCs Dil-acetylated low density lipoprotein (Invitrogen, Carlsbad, CA) and *Bandeiraea simplicifolia* lectin I. Cultured EPCs were subjected to migration analyses by using the chambers, whose upper and lower chambers were separated by a polycarbonate filter (8 μm pore size). Mouse EPCs were resuspended at $5 \times 10^4$/100 μl in EBM-2 BulletKit medium supplemented with 0.5% BSA and were seeded in the upper compartment. Recombinant mouse CCL2 (50 μg/ml), VEGF (100 μg/ml), and GM-CSF (50 μg/ml) were added to the lower compartment. The chambers were incubated at 37°C in 5% $CO_2$ for 12 hours. The cells that had migrated into the lower chamber were counted manually in 5 random high-power

microscopic fields (magnification ×100) in each well. All groups were studied at least in triplicate.

### Statistical analysis

Data were expressed as the mean ± standard error of the mean. For the comparison between normal and diabetic mice or vehicle-treated and CCL2-treated diabetic mice at multiple time points, a 2-way ANOVA followed by Dunnett's post-hoc test was used. To compare the values between two groups, unpaired Student *t* test was performed. $P < 0.05$ was considered statistically significant. All statistical analyses were performed using the Statcel3 software (OMS Publishing, Saitama, Japan) under the supervision of a medical statistician, Dr. Toshio Shimokawa (Wakayama Medical University).

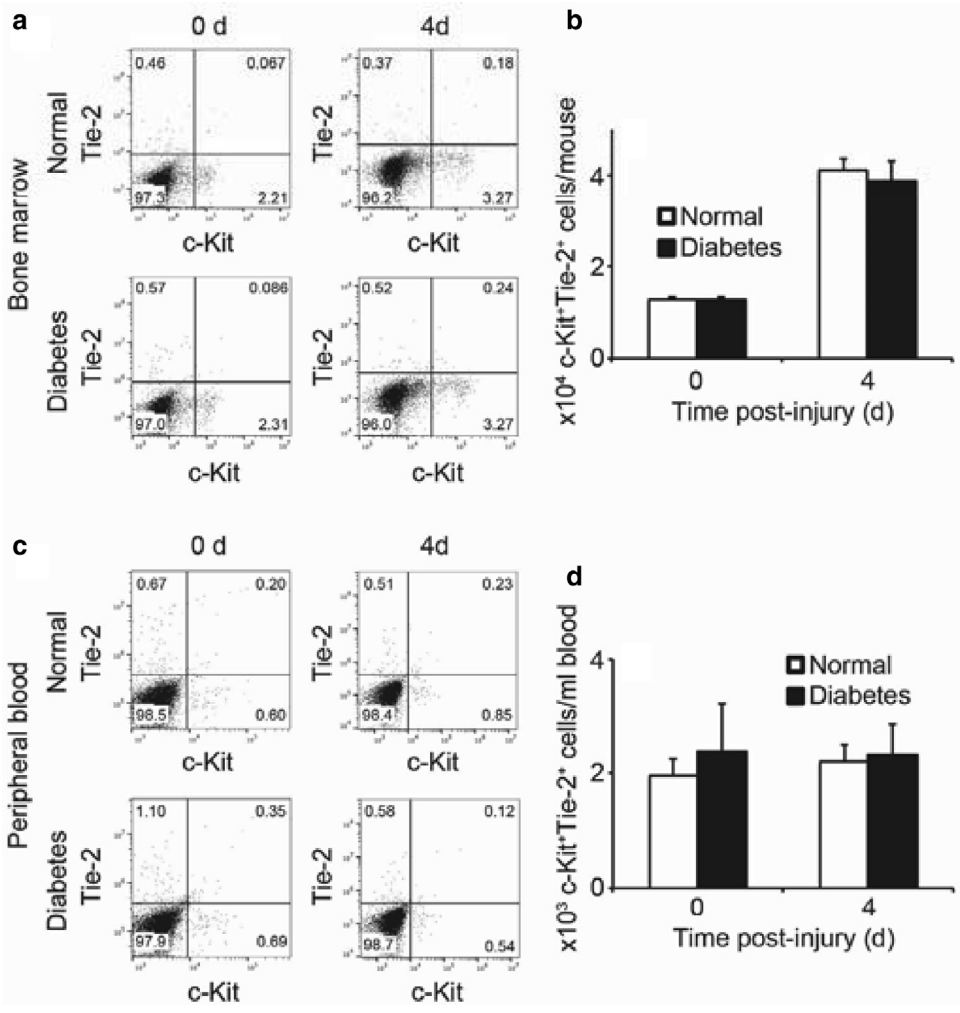


**Supplementary Figure S1. Quantitative evaluation of EPCs after injury in normal mice and mice with diabetes.** (**a**–**d**) bone marrow (a, b) and peripheral blood (c, d) were analyzed to determine $Tie2^+$ $c\text{-}Kit^+$ EPCs; (a, c) flow cytometric analysis; (b, d) number of $Tie2^+$ $c\text{-}Kit^+$ EPCs. Values represent mean ± SEM (n = 6). EPC, endothelial progenitor cell; SEM, standard error of the mean.

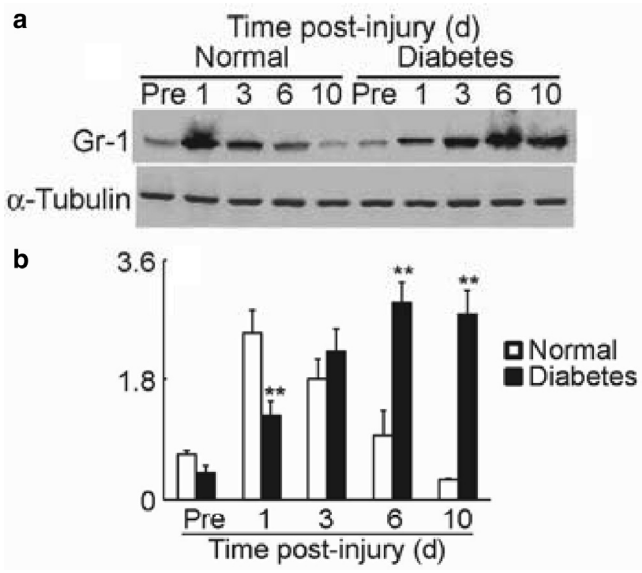


**Supplementary Figure S2. Altered granulocyte recruitment in diabetic mice.** (**a**) Mice were killed 1, 3, 6, and 10 days after wounding. Eight-millimeter diameter biopsy punches were used to collect the injured skin area. Western blotting analysis was carried out using anti-Gr-1 and anti-α-Tubulin mAbs. Representative results from four independent experiments are shown. (**b**) Ratio of Gr-1 to α-Tubulin. All values represent mean ± SEM. **, $P < 0.01$, versus normal mice. SEM, standard error of the mean.

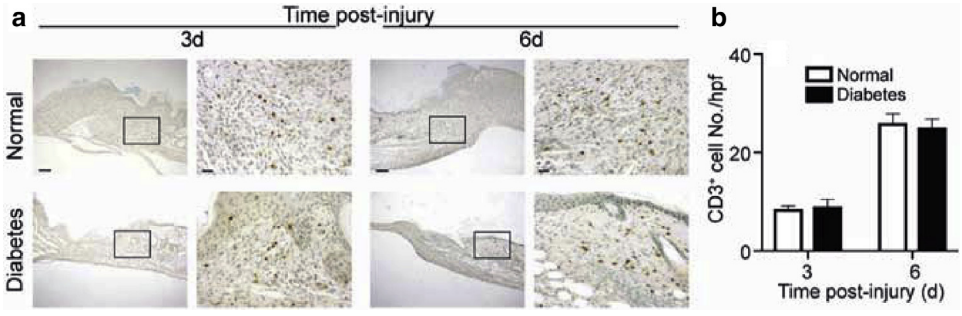


**Supplementary Figure S3. Immunohistochemical analysis with anti-CD3 at wound sites of normoglycemic and diabetic mice.** (**a**) Immunohistochemical detection of $CD3^+$ T cells at wound sites 3 and 6 days after the injury. Representative results from six independent experiments are shown. Scale bars = 100 μm. Scale bars in inserts = 20 μm. (**b**) The number of $CD3^+$ T cells per high-power microscopic field was counted. All values represent mean ± SEM. SEM, standard error of the mean.

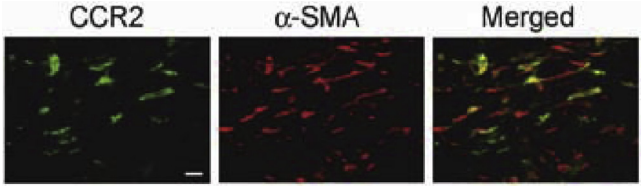


**Supplementary Figure S4. Cell type expressing CCR2.** A double-color immunofluorescence analysis of CCR2-expressing cells in wound sites at 6 days after injury in normal mice. The analysis was performed using anti-CCR2 and anti-α-SMA followed by the observation under a fluorescence microscopy, and signals were merged digitally. Representative results from six individual animals are shown. Scale bar = 20 μm. SMA, smooth muscle actin.

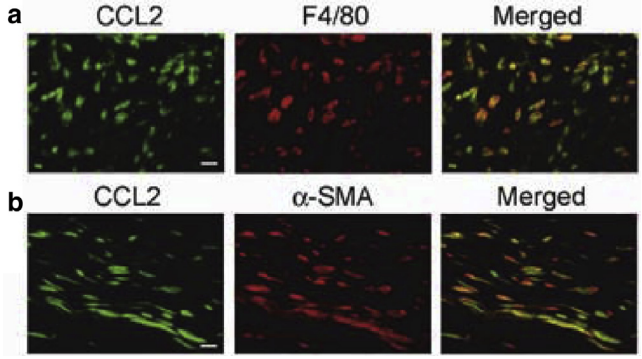


**Supplementary Figure S5. Cell type expressing CCL2. (a, b)** A double-color immunofluorescence analysis of CCL2-expressing cells in wound sites at 6 days after injury in normal mice. The analysis was performed using (a) anti-CCL2 and anti-F4/80 or (b) anti-α-SMA, followed by the observation under a fluorescence microscopy, and signals were merged digitally. Representative results from six individual animals are shown. Scale bars = 20 μm. SMA, smooth muscle actin.

**Supplementary Figure S6. Immunohistochemical analysis with anti-CD3 at wound sites of vehicle- or recombinant CCL2-treated mice with diabetes.** (**a**) Immunohistochemical detection of $CD3^+$ T cells at wound sites 3 and 6 days after the injury. Representative results from six independent experiments are shown. Scale bars = 100 μm. Scale bars in inserts = 20 μm. (**b**) The number of $CD3^+$ T cells per high-power microscopic field was counted.

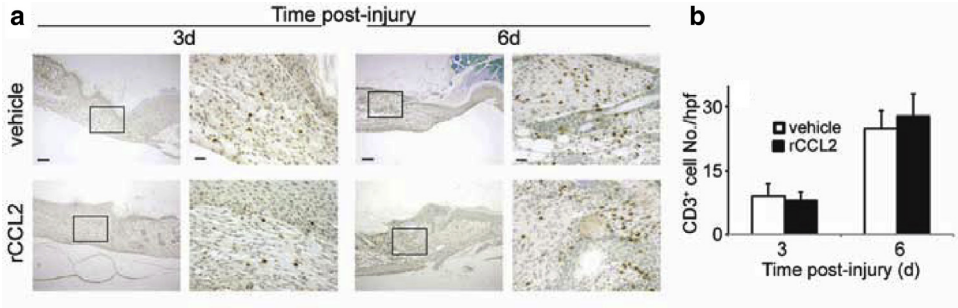


## Supplementary Table S1. Sequences of primers used for real-time RT-PCR

| Transcript | Sequence |
|---|---|
| *Ccl2* | (F)[1] 5′-GCATCCACGTGTTGGCTCA-3′ |
| | (R)[2] 5′-CTCCAGCCTACTCATTGGGATCA-3′ |
| *Tgfb1* | (F) 5′-GTGTGGAGCAACATGTGGAACTCTA-3′ |
| | (R) 5′-TTGGTTCAGCCACTGCCGTA-3′ |
| *Col1a1* | (F) 5′-ATGCCGCGACCTCAAGATG-3′ |
| | (R) 5′-TGAGGCACAGACGGCTGAGTA-3′ |
| *Vegf* | (F) 5′-TCCAACATCACCATGCAGAT-3′ |
| | (R) 5′-CATCTGCAAGTACGTTCGTT-3′ |
| *Actb* | (F) 5′-CATCCGTAAAGACCTCTATGCCAAC-3′ |
| | (R) 5′-ATGGAGCCACCGATCCACA-3′ |

Abbreviation: RT-PCR, reverse transcriptase–PCR.
[1]Forward primer.
[2]Reverse primer.